



A new global dataset of photosynthesis parameters

Žarko Kovač¹, Marija Baćeković Koloper^{1*}, Shubha Sathyendranath^{2,3}, Gemma Kulk^{2,3},
Heather Bouman⁴, Leon Ćatipović¹

¹*Faculty of Science, University of Split, Rudera Boškovića 33, 21000 Split, Croatia*

²*Plymouth Marine Laboratory, Prospect Place, The Hoe, Plymouth PL1 3DH, UK*

³*National Centre for Earth Observations, Plymouth Marine Laboratory, Prospect Place, The Hoe, Plymouth PL1 3DH, UK*

⁴*Department of Earth Sciences, University of Oxford, Oxford, OX1 3AN, UK*

*corresponding author: mbacekovi@pmfst.hr

Abstract

Photosynthesis-irradiance and photosynthesis-depth experiments are two standard ways of experimentally quantifying primary production. These measurements have historically formed the backbone for the formulation of mathematical models of primary production and to this day remain an invaluable resource for model development and refinement. From such experiments information on photosynthesis parameters can be extracted, which allows for the quantification of the photosynthesis light dependence, essential in the calculation of primary production. To this day, this is the only avenue for photosynthesis parameters estimation, making such data invaluable for primary production modelling. In the literature, there have been several efforts to form global datasets of photosynthesis parameters, collected at various sites across the world oceans and seas. Here, we use a publicly available global dataset of in situ primary production profiles and construct a new database of photosynthesis parameters. We use an inverse modelling approach that is described in great details, along with the data requirements. For a forward model, we employ a fully solvable analytical model of the production profile, and we use the inverse model to compare it with the measured production profile, while constraining it with measured daily watercolumn production. Using this approach, we successfully recovered 4160 photosynthesis-irradiance parameters from the global oceans, which enabled a model versus data comparison for watercolumn production. The spatio-temporal distribution of the new dataset is presented and compared to existing datasets. Finally, the new photosynthesis parameters dataset is provided publicly, along with metadata needed for the implementation in primary production models.

Keywords: primary production, photosynthesis parameters, parameter estimation, global dataset

1 Introduction

Estimation of global marine primary production is an ongoing pursuit of biophysical oceanography (Brewin et al., 2023) and over time a number of models and algorithms have been developed to tackle this problem (Platt & Sathyendranath, 1988; Balch et al., 1992; Antoine et al., 1996; Campbell et al., 2002; Buitenhuis et al., 2013). Modern global state of the art models of marine primary production require four essential sources of information as a minimum: surface photosynthetically active radiation, attenuation coefficients for downwelling radiance, chlorophyll concentration and photosynthesis



parameters (Kulk et al., 2020, 2021; Westberry et al., 2023). Photosynthetically active radiation is readily available as data products on a global scale, or is easily measurable in situ via radiometers. The same would hold for the attenuation coefficient. Depending on the complexity of the models, namely being spectrally resolved or not and on whether the model admits vertical structure in phytoplankton or not (Sathyendranath & Platt, 1989a; Kyewalyanga et al., 1992), data requirements on surface photosynthetically active radiation and attenuation coefficients vary significantly (Platt et al., 2017). Global scale chlorophyll concentration for the surface ocean is typically estimated by using remotely sensed radiance data, since the time of the seminal paper by Gordon et al. (1983), whereas locally it can be estimated by a variety of observational methods. The final requirements for model implementation are values of photosynthesis parameters, information on which is only available, to this date, via direct measurements at sea. Estimation of these parameters via remote sensing still eludes us (but see Topliss & Platt (1986)) and that is why such datasets (Bouman et al., 2018; Kulk et al., 2020, 2021) are an invaluable resource for primary production models. They also help constrain the magnitude of global primary production (Richardson et al., 2016), an important flux in the global carbon budget (Friedlingstein et al., 2024).

In all classes of models, surface irradiance is used as the energy source to drive photosynthesis (Platt & Sathyendranath, 1993; Behrenfeld & Falkowski, 1997a). A light penetration model is used to calculate the underwater light field, in combination with a model for the prescription of the chlorophyll profile (Platt & Sathyendranath, 1991). Depending on the complexity of the model, the effect of chlorophyll on the underwater light field may be included in the model (Sathyendranath & Platt, 1989b). However, knowing the chlorophyll concentration at a given depth, along with the available light, is not enough to calculate the carbon uptake through photosynthesis. The final step is achieved by using photosynthesis-irradiance functions (Platt et al., 1977; Jones et al., 2014), which themselves link chlorophyll, a state variable, with primary production, a flux, for a given irradiance level (Amirian et al., 2025). By integrating the flux of carbon through photosynthesis over time, typically one day, and over depth, the models arrive at an estimate of primary production per unit ocean surface (Platt et al., 1991). By subsequently integrating over the ocean surface the models arrive at a global estimate of primary production, and further integration over the course of one year yields an annual estimate of primary production (Longhurst et al., 1995; Buitenhuis et al., 2013).

To make the models precise, information on the rate of primary production as a function of light is essential. This is provided by the photosynthesis-irradiance functions, the exact value of which is determined by the values of photosynthesis parameters (Gallegos & Platt, 1981). Direct estimation of photosynthesis parameters is based on costly and scarce field measurements of carbon assimilation by phytoplankton in labelled carbon experiments carried out in vitro, under controlled light conditions (Platt & Jassby, 1976; Bouman et al., 2018). A relatively novel method applies inverse modelling techniques to data from in situ incubations under natural light conditions (Kovač et al., 2016b). The in situ experiments are typically even more expensive and time consuming than direct photosynthesis-irradiance experiments, and the inverse modelling technique serves to extract additional information from them, and to fill gaps in the direct measurements of photosynthesis-irradiance experiments.

The photosynthesis-irradiance experiments provide information on the rate of carbon assimilation as a function of irradiance, and parameter estimation is carried out by first selecting a photosynthesis irradiance function, followed by fitting it to the data (Jassby & Platt, 1976). The results yield best estimates of photosynthesis parameters. The controlled nature of the experiments, and the availability of a large parameter dataset was highly valuable, in that it provided the backbone for the formulation of primary production models based on first principles (Platt et al., 1988, 1990). The latest published archive of photosynthesis parameters estimated in such a way holds 5 711 estimated values of photosynthesis parameters from around the global ocean (Bouman et al., 2018). These parameters (or earlier subsets of the data) are routinely used in global models of primary production (Longhurst et al., 1995; Kulk et al., 2020, 2021).



69 The other set of measurements routinely performed at sea is the in situ implementation of the carbon assimilation
70 method (Strickland & Parsons, 1972; Peterson, 1980; Behrenfeld & Falkowski, 1997b). These measurements provide
71 information on the vertical structure of primary production (often reported as daily rates), the so called production
72 profile. Measured production profiles have not been used routinely to derive photosynthesis parameters, until suitable
73 methods emerged (Kovač et al., 2016b). These methods use inverse modelling to find the optimal values of photosynthesis
74 parameters based on measured production profiles and have been successfully tested at two time series stations: Hawaii
75 Ocean Time Series (Kovač et al., 2016a) and Bermuda Atlantic Time Series Study (Kovač et al., 2018).

76 One major obstacle with using these datasets more to extract photosynthesis parameters might have been that they
77 were dispersed over various data repositories, and not readily accessible. However, due to the recent work by Mattei
78 & Scardi (2021), a vast collection of in situ data with 6084 primary production profiles has been assembled under one
79 umbrella. The dataset contains information on measured primary production profiles along with chlorophyll profiles,
80 surface photosynthetically active radiation and the attenuation coefficient for underwater irradiance. These are the
81 essential variables needed to estimate photosynthesis parameters from in situ production profiles via inverse modelling
82 (Kovač et al., 2017b). Therefore, having these data at hand implies there is a potential for the estimation of photosynthesis
83 parameters from all these profiles, under the assumption that the inverse modelling procedure is successful in estimating
84 the parameters from each measured production profile. Precisely this is explored in this paper.

85 We first describe the inverse modelling methodology used to estimate the photosynthesis parameters from in situ
86 production profiles. Subsequently, we describe the dataset, from the point of view of data needed for photosynthesis
87 parameters estimation. Limitations of both the inverse model and the dataset are discussed, with details on the forward
88 and the inverse models provided in the Appendices. Model data comparisons are made for production at depth and for
89 watercolumn production. Finally, the new global database of photosynthesis parameters is made freely available online,
90 along with the codes for data access.

91 2 Inverse model

92 A canonical model for daily watercolumn primary production is based on an assumption of a functional dependence
93 between available light and the rate of carbon assimilation by photosynthesis (Platt & Sathyendranath, 1991). This
94 functional dependence is expressed mathematically with the photosynthesis-irradiance functions (Jassby & Platt, 1976),
95 which state the rate of carbon assimilation P per unit biomass B as a function of irradiance I :

$$P^B = p^B(I), \quad (1)$$

96 where P^B is the biomass normalised production and the notation p^B marks the photosynthesis irradiance function (Figure
97 1). There are numerous such functions in oceanographic usage, with a rich history of applications (Zonneveld, 1998; Kovač
98 et al., 2017b). All functions are expressible using two parameters: the initial slope α^B and the assimilation number P_m^B
99 (Platt et al., 1977; Frenette et al., 1993; Behrenfeld et al., 2004), which we write as:

$$P^B = p^B(I | \alpha^B, P_m^B). \quad (2)$$

100 Here, the initial slope α^B describes the linear response of primary production at low light, whereas the assimilation
101 number P_m^B describes the rate of primary production at saturating light intensities (MacIntyre et al., 2002; Falkowski,
102 1981; Milligan et al., 2015). In the ocean, irradiance is a function of both depth z and time t and a light penetration
103 model is required to calculate $I = I(z, t)$ (Kirk, 2011). Keeping in mind the limitations of the Mattei & Scardi (2021)
104 dataset, namely a single value for the attenuation coefficient K and a single value for noon irradiance I_0^m , we employ a

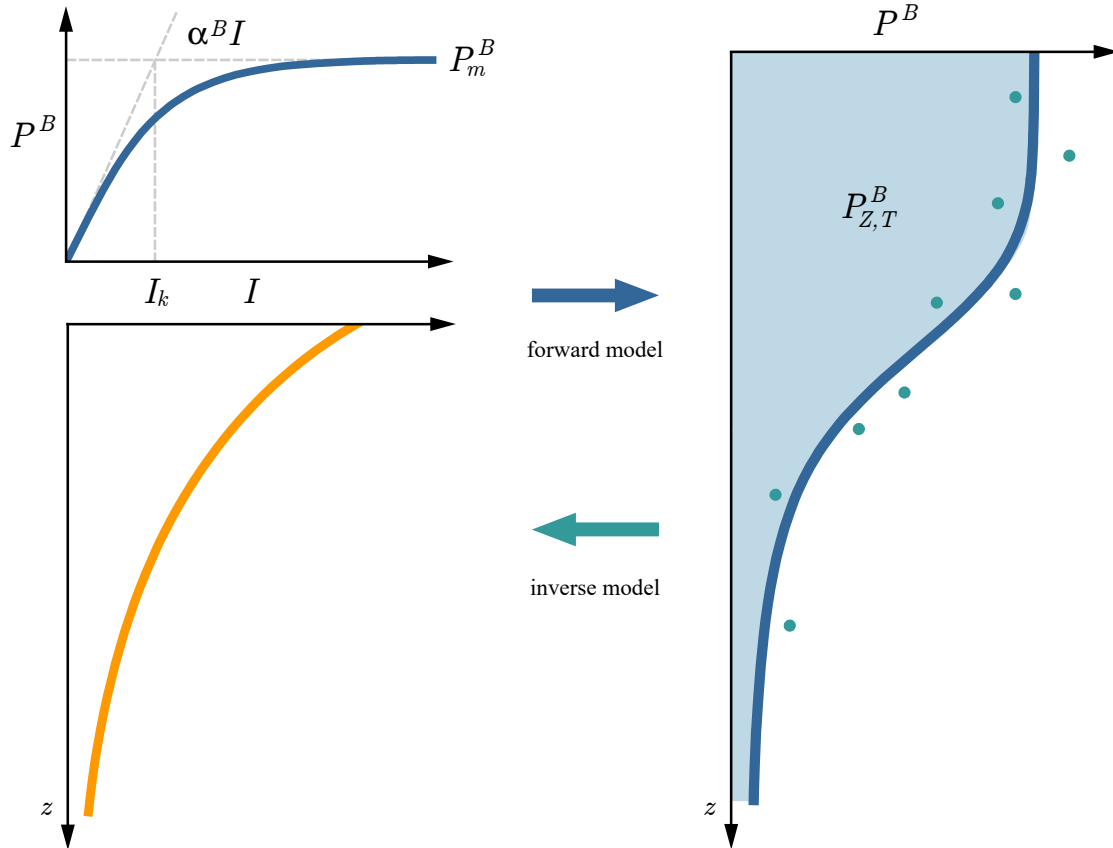


Figure 1: Graphical representation of the relation between the forward and inverse models. Both models are based on a functional relationship between production and light, expressed using photosynthesis irradiance functions (top left). These functions require information on the photosynthesis parameters: the initial slope α^B and the assimilation number P_m^B , which are typically estimated from in vitro photosynthesis irradiance experiments. With information on the biomass profile and underwater irradiance (orange curve, bottom left) a forward model calculates the daily production profile (blue curve on the right) and watercolumn production (blue surface on the right). An inverse model does the opposite. With an in situ measured production profile (green dots) an inverse model estimates the values of the photosynthesis parameters by minimizing the error between the model prediction (blue curve) and the measurements (green dots).

105 relatively simple light penetration model:

$$I(z, t) = I_0^m \sin(\pi t/D) \exp(-Kz), \quad (3)$$

106 where D is daylength (time from sunrise till sunset). Knowing the underwater irradiance (3) and the response of primary
 107 production to it (2), enables the calculation of primary production per unit biomass, for a given depth and time, as
 108 $P^B(z, t) = p^B(I(z, t))$. To calculate primary production, additional information on biomass at depth is needed, which
 109 is specified as $B(z)$, and typically taken as constant during one day (but see Kováč et al. (2017a)). Multiplication of
 110 normalized production by biomass and integration over daylength yields the daily production profile $P_T(z)$:

$$P_T(z) = B(z) \int_0^D p^B(I(z, t)) dt, \quad (4)$$



111 which is the model analogue of the in situ measured production profile (Kovač et al., 2016a). By further integration over
 112 depth we obtain daily watercolumn production as:

$$P_{Z,T} = \int_0^{\infty} P_T(z) dz. \quad (5)$$

113 The two integrals are typically solved numerically, but for the Platt et al. (1980) photosynthesis irradiance function, both
 114 have been solved analytically. The exact solution for watercolumn production with uniform biomass is provided by Platt
 115 et al. (1990), whereas solutions for the case of non-uniform biomass profiles can be found in Kovač et al. (2017a). The
 116 analytical solution for the daily production profile is given in Kovač et al. (2016a), with a summary of other analytical
 117 solutions provided by Kovač et al. (2017b). In the context of parameter estimation both (4) and (5) would be referred
 118 to as forward models, in the sense that for given parameter values the model calculates a primary production profile
 119 and watercolumn production (Figure 1). The opposite procedure to this, namely estimation of parameters from a known
 120 production profile, is referred to as an inverse procedure, or an inverse model (Figure 1). Details of the forward and
 121 inverse models used in this study are given in Appendix A and Appendix B, respectively.

122 To extract the values of photosynthesis parameters given a measured in situ production profile, we first normalize the
 123 production profile (4) with biomass, to get at the normalised daily production profile (Kovač et al., 2016a), which we
 124 recognize is also a function of parameter values themselves, written in analogy with (2), as:

$$P_T^B(z) = P_T^B(z | \alpha^B, P_m^B). \quad (6)$$

125 Now, for a given survey from the Mattei & Scardi (2021) dataset we obtain by measurement the following variables:
 126 chlorophyll profile $\tilde{B}(z_n)$ and daily production profile $\tilde{P}_T(z_n)$, both at a sequence of depths z_n , along with noon irradiance
 127 \tilde{I}_0^m and the attenuation coefficient \tilde{K} , complemented with daylength \tilde{D} . We use the tilde \sim to indicate a measured variable,
 128 whereas without tilde, the variable refers to the model.

129 To be more precise, from measurements we obtain, for a given survey, a sequence of pairs: $\tilde{B}(z_n)$ and $\tilde{P}_T(z_n)$, at
 130 depths z_n , with $n = 1, 2, \dots, N$, and N being the total number of measurement depths for a given survey. For each depth
 131 z_n , by dividing measured daily production $\tilde{P}_T(z_n)$ by the measured biomass, $\tilde{B}(z_n)$ we get the measured normalised daily
 132 production profile as:

$$\tilde{P}_T^B(z_n) = \tilde{P}_T(z_n) / \tilde{B}(z_n). \quad (7)$$

133 To estimate the values of photosynthesis parameters, the model normalised production profile (6) is compared with the
 134 measured normalised production profile (7). To help constrain the model we also compare the modelled and measured
 135 normalised watercolumn production. Model normalised watercolumn production is given as:

$$P_{Z,T}^B = \int_0^{\infty} P_T^B(z) dz, \quad (8)$$

136 and measured normalised watercolumn production as:

$$\tilde{P}_{Z,T}^B = \sum_{n=1}^N \tilde{P}_T^B(z_n) \Delta z_n, \quad (9)$$

137 where Δz_n is the depth interval associated with each measurement depth (see Appendix A and Appendix B). Quantifi-
 138 cation of the model data mismatch is defined with the following optimal function as:

$$\begin{aligned} \mathcal{P}(\alpha^B, P_m^B) = & \sum_{n=1}^N \left(P_T^B(z_n | \alpha^B, P_m^B) - \tilde{P}_T^B(z_n) \right)^2 \\ & + \left(P_{Z,T}^B(\alpha^B, P_m^B) - \tilde{P}_{Z,T}^B \right)^2, \end{aligned} \quad (10)$$

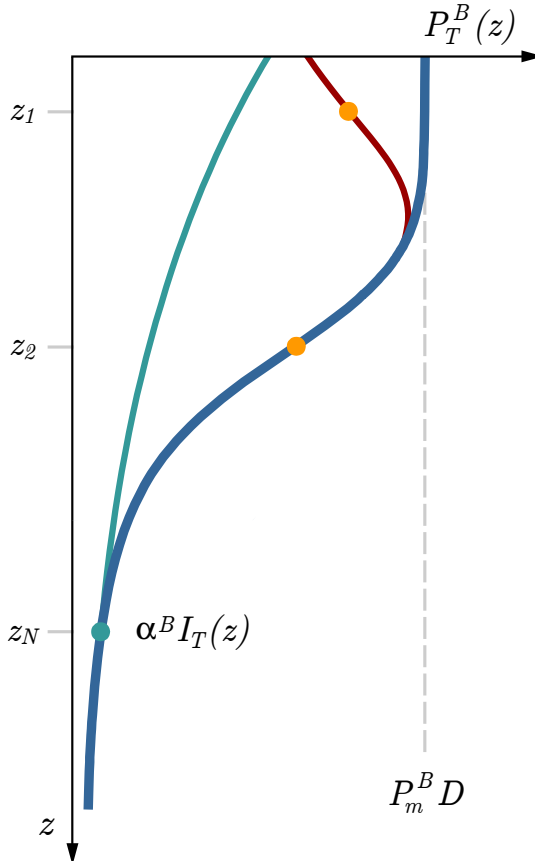


Figure 2: The starting estimate for the value of the assimilation number can be estimated from measured surface values of primary production by assuming saturation close to the surface (grey dashed line). The in situ production measurements carried out close to the ocean surface (orange dot at depth z_1) may experience photoinhibition due to exposure to high irradiance (irradiance profile given in green). This will cause a dip in the production profile (red curve) close to the surface from what would otherwise be a saturating profile (blue curve). Likewise, the starting estimate for the initial slope can be estimated from measurements at great depth where saturation of photosynthesis does not take place during the experiment (green dot).

which is a function of photosynthesis parameters. The first term takes into account the shape of the measured production profile (green dots on the right in Figure 1), while the second term takes into account normalised watercolumn production (blue surface on the right in Figure 1). Now, the problem of estimating photosynthesis parameters from measured production profiles is reduced to finding the minimum of this function (Kovač et al., 2016a,b). Optimization methods for achieving this, as well as the technical details of the forward and inverse model are provided in Appendix A and Appendix B. The inverse model is applied for each profile on its own, from which photosynthesis parameters are estimated. We label the estimated values of photosynthesis parameters as: $\hat{\alpha}^B$ and \hat{P}_m^B . This procedure is repeated over the entire Mattei & Scardi (2021) dataset, which yields the new dataset of photosynthesis parameters. But prior to the application, we first describe the limitations of the approach, which stem from data and model limitations.

The strongest limitation on the inverse approach comes from the assumption of vertical homogeneity in photosynthesis parameters. This implies that one value of the initial slope α^B and one value of the assimilation number P_n^B is assigned to phytoplankton throughout the entire water column. In the ocean, photosynthesis parameters may, and likely do vary vertically, especially in case of strong stratification (Bouman et al., 2018). Also, temporally, phytoplankton are known



152 to adjust values of photosynthesis parameters over the course of a few generations (Reynolds, 2006). However, the time
 153 scale of in situ incubations is of the order of one day, therefore it is unlikely that significant changes will occur within
 154 the duration of the experiment. In principle, if there were numerous measurements carried out in the vertical, such
 155 that the production and biomass profiles were resolved well vertically, a more complex model with vertically varying
 156 photosynthesis parameters could be used. The same reasoning would apply if numerous shorter incubations were carried
 157 out during the day.

158 A direct mathematical consequence of vertically uniform photosynthesis parameters is the constraints on the applica-
 159 tion range of the model. In the case of uniform photosynthesis parameters, the normalised daily production profile is a
 160 declining function of depth (Figure 2):

$$\frac{\partial P_T^B(z)}{\partial z} < 0. \quad (11)$$

161 Therefore, the model can only be expected to work well for in situ normalised production profiles which also decline with
 162 depth. This is easy to test by simply observing whether:

$$\tilde{P}_T^B(z_n) > \tilde{P}_T^B(z_{n+1}). \quad (12)$$

163 We should also stress that measurements near the surface, as shown in Figure 2, may be prone to photoinhibition: a
 164 reduction of primary production at high irradiance (Marshall et al., 2000). The reduction of primary production due to
 165 photoinhibition is likely to occur if the incubations are carried out for prolonged periods of time under high irradiance
 166 (Ross et al., 2011b,a). In the ocean, phytoplankton are free floating and are continually being circulated in the mixed
 167 layer, whereas for in situ incubations the experiments are carried out at fixed depths. This implies mixing is prevented
 168 and phytoplankton which would otherwise be freely mixed, are now exposed to significantly higher irradiance, which may
 169 lead to light stress. Signs of photoinhibition are easily observed in the normalised production profile by testing whether
 170 normalised daily production at the first measurement depth is less than that measured at the subsequent depths (Figure
 171 2). Given that photoinhibition occurs close to the surface, its effect on watercolumn production is expected not to be
 172 pronounced (Platt et al., 1990; Ross et al., 2011b).

173 Further more, to enable faster and more accurate estimation of optimal photosynthesis parameters, initial values in
 174 the optimization procedure need to be specified (Kovač et al., 2016b). For the initial value of the assimilation number,
 175 we note first that saturation of photosynthesis is more likely close to the surface, but not at the first measurement depth,
 176 since that is where photoinhibition might occur. At the second measurement depth, it is more likely that photoinhibition
 177 will not be pronounced and we can assume that during most of the incubation's duration primary production at this
 178 depth will be close to saturation for most of the day, except when light levels drop towards zero at dawn and dusk (Figure
 179 2). Therefore, we can approximate daily normalised production at the second depth as:

$$\tilde{P}_T^B(z_2) \approx P_m^B D. \quad (13)$$

180 This assumption leads easily to the starting value for the assimilation number (Figure 2), which we label as $(P_m^B)_0$:

$$(P_m^B)_0 = \frac{\tilde{P}_T^B(z_2)}{D}. \quad (14)$$

181 Likewise, the starting value of the initial slope can also be approximated from the production profile. At great depth,
 182 photosynthesis will likely remain unsaturated for the duration of the incubation and production will depend on irradiance
 183 linearly. This implies that we can approximate daily normalised production at the final depth z_N , provided it is optically
 184 deep enough, as:

$$P_T^B(z_N) \approx \alpha^B I_T e^{-K z_N}, \quad (15)$$

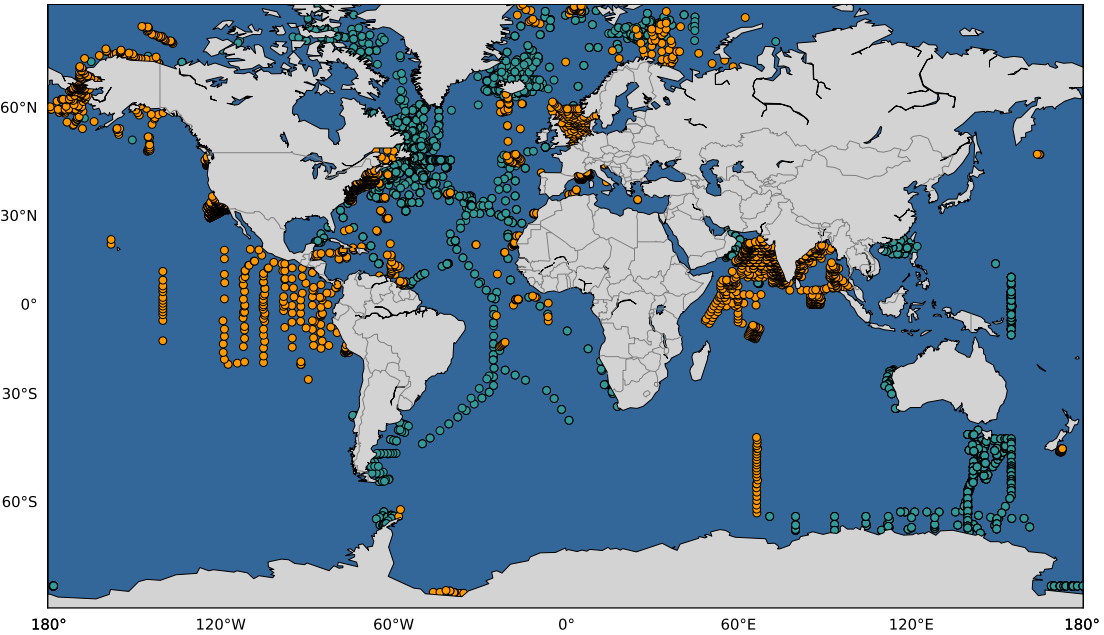


Figure 3: Map of the in situ production profiles from the Mattei & Scardi (2021) dataset (orange dots). In total there are 6 084 chlorophyll and production profiles in the dataset. Most of the data come from the Northern Hemisphere. The data were collected from 1958 till 2017, with the total of 37 722 individual measurements of chlorophyll and primary production pairs. Also shown is the published archive of photosynthesis parameters by Bouman et al. (2018), which contains 5 711 values of photosynthesis parameters globally in the time span from 1977 to 2013 (green dots). The Mattei & Scardi (2021) dataset complements the Bouman et al. (2018) dataset by covering areas in which no photosynthesis parameters were published, creating an incentive for photosynthesis parameters estimation from in situ production profiles.

185 where I_T is the daily integral of surface irradiance (Figure 2). From this we can express the starting value of the initial
 186 slope as:

$$(\alpha^B)_0 = \frac{P_T^B(z_N)}{I_T e^{-Kz_N}}. \quad (16)$$

187 Having the starting values for both the assimilation number and the initial slope, helps speed up the search process for
 188 the optimal parameter values. It also aids in preventing the optimization algorithm from ending up in a local minima of
 189 the error function (10), instead of the global minima. With the inverse model described, we now proceed to describe the
 190 dataset.

191 3 Production profiles dataset

192 The Mattei & Scardi (2021) dataset contains primary production profiles measured in situ and distributed throughout
 193 the global ocean as shown in Figure 3. The authors have compiled the dataset by complementing the already existing
 194 dataset from the Oregon State University, which at the time was consisted of 2214 production profiles. This dataset was
 195 used in the development of the Vertically Generalized Production Model (Behrenfeld & Falkowski, 1997a,b). It was then
 196 supplemented by Mattei & Scardi (2021) with additional 3870 profiles from the world oceans.

197 The Mattei & Scardi (2021) dataset contains 6084 individual production profiles measured from 1958 till 2017, with
 198 the total of 37722 individual pairs of measurements of primary production and chlorophyll. The vast majority (5 578) of
 199 the profiles are from the Northern Hemisphere (Figure 3), whereas only 478 are located in the Southern Hemisphere. Over
 200 the seasonal cycle, the authors report: 1701 for winter, 1802 for spring, 1589 for summer and 992 for autumn, which is



201 a relatively uniform annual coverage. The full dataset contained 3755 profiles with measured surface photosynthetically
202 active radiation (PAR), whereas the missing PAR were filled with satellite estimates (see Mattei & Scardi (2021) for
203 details). PAR was provided in units of $\text{E m}^{-2}\text{d}^{-1}$ and the conversion to W m^{-2} was done using Smith and Morel's
204 procedure (Morel & Smith, 1974). Surface noon irradiance I_0^m was subsequently determined as $\tilde{I}_0^m = \tilde{I}_T \pi / 2D$, where \tilde{I}_T
205 is the total received irradiance during daylength. Note that this conversion assumes a sine function for the time-dependent
206 variation of irradiance over the daylength, which is consistent with the model used here, namely equation (3) (see also
207 Platt et al. (1990)). For the profiles without measured PAR, Mattei & Scardi (2021) have performed gap filling from 2003
208 onwards. The authors have also performed gap filling of missing chlorophyll and production data with depth weighted
209 averages of the closest measured values.

210 For each primary production profile the authors provided numerous associated variables and metadata, but we focus
211 solely on the ones needed for photosynthesis parameters estimation using the above-described inverse model. The essen-
212 tial variables needed to estimate photosynthesis parameters from in situ experiments are: chlorophyll profile, primary
213 production profile, surface photosynthetically active radiation and the diffuse attenuation coefficient for downwelling
214 irradiance. These are all given in the dataset. To be more precise, the euphotic zone depth Z_e is given in the dataset,
215 with the calculation of the attenuation coefficient done simply as $\tilde{K} = \ln(100)/Z_e$.

216 The dataset also contains auxiliary variables for each experiment, such as: day, month, year, latitude and longitude,
217 euphotic zone depth, mixed layer depth, bottom depth, distance from coastline, as well as many other variables. See the
218 Supplementary material from the Mattei & Scardi (2021) paper for details on the dataset. The full dataset is available
219 on the PANGAEA repository via the following link: <https://doi.pangaea.de/10.1594/PANGAEA.932417>.

220 The auxiliary variables enable us to ascertain the adequacy of the dataset for the inverse model. From the standpoint
221 of photosynthesis parameter estimation, it is important to know the range of irradiance experienced by the phytoplankton
222 during the incubations (Kovač et al., 2016b), which can be ascertained by expressing the measurement depth of each
223 experiment as an optical depth ζ , as shown in Figure 4.a. From the distribution of the measurement frequency as a
224 function of optical depth we observe that most of the measurements are carried out at shallow optical depths. As the
225 optical depth increases the number of measurements drops off. This is expected, given primary production measurements
226 are typically performed within the euphotic zone (corresponding to $\zeta = 4.6$).

227 In fact, after the estimation of optimal photosynthesis parameters, it is possible to partition the water column into
228 depths for which $I(z) > I_k$, and depths for which $I(z) < I_k$. Nominally, for depths that meet the first criterion, production
229 would be determined by P_m^B , and for the latter case, production would be determined by α^B (Kovač et al., 2016b). From
230 the limited case of application to computation of water-column production (which is the case dealt with, here), the
231 importance is to get P_m^B right for depths that lie above the $I(z) = I_k$ depth horizon, and to get α^B right for depths below
232 that horizon. For this reason it is important that the incubations are carried out over a range of optical depths.

233 Another important indicator for inverse model applicability is the value of the mixed layer depth relative to euphotic
234 depth for each station, shown in Figure 4.b. Here we observe that for most of the profiles mixed layer depth was of the
235 same order of magnitude as the euphotic depth. This implies probable vertical homogeneity in photosynthesis parameters
236 for the given incubations. The highest number of profiles has the mixed layer depth almost equal to the euphotic depth,
237 which is also a good indicator for the justification of vertical homogeneity of photosynthesis parameters.

238 Finally, for the inverse model to be able to estimate the values of photosynthesis parameters, the measured production
239 profile has to have a minimal number of depths to vertically resolve the shape of the normalised production profile. As
240 demonstrated by Kovač et al. (2016b) the normalised production profile (6) is uniquely determined by the photosynthesis
241 parameters, whereas normalised daily watercolumn production (8) is not. This is because the normalised watercolumn
242 production is an integral of the normalised production profile (Figure 1) and therefore loses the degrees of freedom that

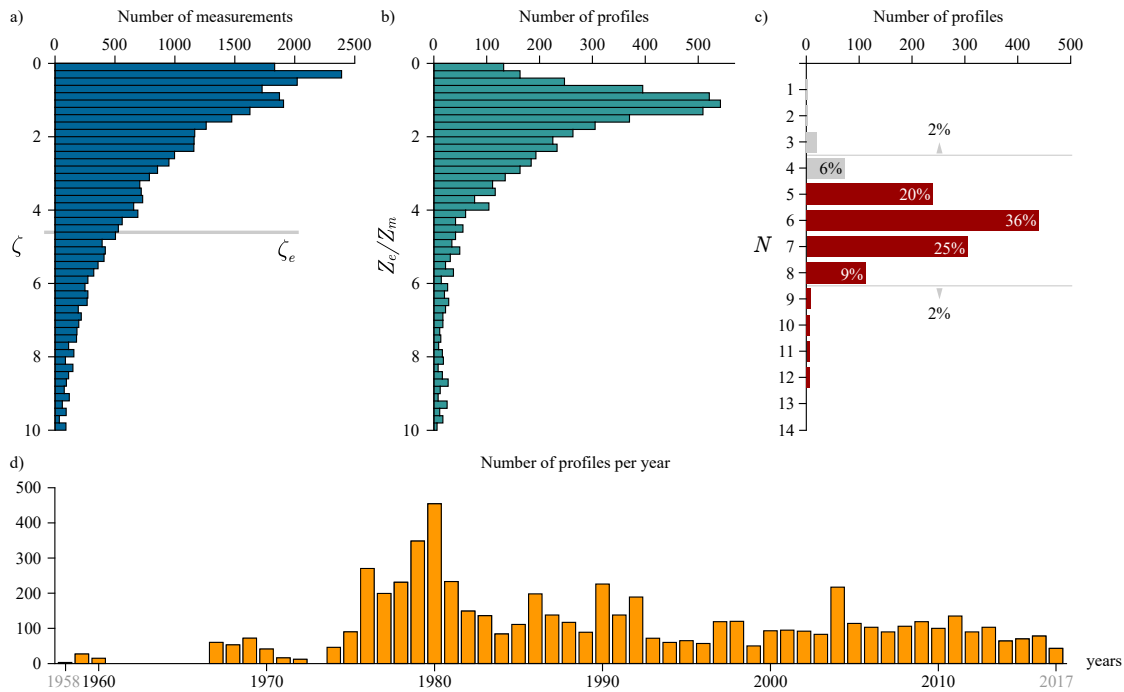


Figure 4: Plots of auxiliary variables. a) Histogram of measurement depths expressed as optical depths. Each individual measurement is treated as one entry. Euphotic zone ζ_e is highlighted by the grey line. b) Histogram of the ratio between the euphotic depth and the mixed layer depth. Here each profile is treated as one entry. c) Histogram of profiles with a given number of measurement depths. The two grey arrows indicate that percentages refer to all the profiles below or above the grey line. d) Time series of the number of measured production profiles per year globally.

243 are present in the production profile, which enable the estimation of photosynthesis parameters. Therefore, a given pair
 244 of photosynthesis parameters may not be an exact match for the normalised production profile, but it may be a good
 245 match for watercolumn production.

246 We have analysed the distribution of profiles with respect to the number of measurement depths per profile, as shown
 247 in Figure 4.c. The highest number of profiles has 6 measurement depths, which is adequate for successful parameter
 248 estimation. The total number of profiles with 6 or more measurement depths accounts for 72% of the measured profiles.
 249 Around 20% of the profiles have 5 measurement depths, which is on the limit for successful parameter estimation. In
 250 order to use as much of the available data as possible, we have opted to use these profiles as well in parameter estimation.
 251 The remainder 8% of profiles have less than 5 measurement depths. In other words, out of the 6 084 profiles, 473. For
 252 these profiles, it is not feasible to estimate both parameters, and therefore we opted to exclude them. On the other end,
 253 some profiles have measurements from 9 to 14 depths (which is excellent), but these account for less than 2% of all the
 254 profiles.

255 Looking at the temporal distribution of measurements, as shown in Figure 4.d, the observations start in 1958, but
 256 there is a gap from 1961 till 1966, with another gap year in 1973. After 1975, there is a surge in data collection, with
 257 the highest number of profiles being measured in 1980 and in the neighbouring years. Afterwards, the global number of
 258 measured profiles is of the order of 100 per year. This is arguably very low, highlighting the value of such measurements,
 259 given the high demand for photosynthesis parameters in remote sensing applications and in ecosystem models. With this
 260 in mind, we now proceed to describe the application of the inverse model and the obtained results.



261 4 Results

262 As a first step in the application of the inverse model we have analysed primary production profiles for signs of vertical
263 homogeneity in photosynthesis parameters, by testing whether they meet condition (12), and if so for how many depths.
264 Out of the total 5611 profiles with more than 4 measurement depths, 988 profiles do not violate this condition at all, 2407
265 profiles violate it at one depth, 1469 at two depths and 747 at three or more depths. We have at first applied the inverse
266 model on all profiles only to find that those profiles which strongly violate the vertical homogeneity condition result in
267 outlier values for photosynthesis parameters. Therefore, we focus on those profiles for which the vertical homogeneity
268 condition is not violated, or violated at one or two depths. In total there are 4864 such profiles. This accounts for 80%
269 of the original 6084 profiles in the Mattei & Scardi (2021) dataset.

270 Distributions of photosynthesis parameters obtained from these profiles are provided in Figure 5. The obtained pa-
271 rameter values are within the expected ranges thus far reported in the literature (Kovač et al., 2017b; Bouman et al., 2018;
272 Amirian et al., 2025). The estimated values of the initial slope α^B range from above 0 to 0.6 mg C (mg Chl) $^{-1}$ (W m $^{-2}$) $^{-1}$ h $^{-1}$,
273 with only a handful parameter values above the upper limit. The majority of values of the assimilation number P_m^B are
274 found to be below 10 mg C (mg Chl) $^{-1}$ h $^{-1}$, with the bulk of the estimates being above 0 and below 5 mg C (mg Chl) $^{-1}$ h $^{-1}$,
275 consistent with conventional photosynthesis-irradiance experiments. Neither of these parameters are normally distributed,
276 being positively skewed and exhibiting long tails. The mean and median of the initial slope α^B being 0.194 and 0.130
277 mg C (mg Chl) $^{-1}$ (W m $^{-2}$) $^{-1}$ h $^{-1}$, respectively, with the mean and median of the assimilation number P_m^B being 4.315
278 and 2.736 mg C (mg Chl) $^{-1}$ h $^{-1}$, respectively. From the information on the values of the initial slope and the assimilation
279 number it is straightforward to calculate the photoadaptation parameter, defined as:

$$I_k = \frac{P_m^B}{\alpha^B}. \quad (17)$$

280 The photoadaptation parameter describes how phytoplankton adjust their light-harvesting capacity to ambient light
281 conditions (Reynolds, 2006; Kirk, 2011). It represents the irradiance at which phytoplankton transition from light limited
282 to light saturated photosynthesis (Jassby & Platt, 1976) and is also a measure of the light level to which phytoplankton
283 have adapted (Zonneveld, 1997). Distribution of the photoadaptation parameter is also given in Figure 5. It is positively
284 skewed with a long tail. The bulk of the photoadaptation parameter values are found below 50 W m $^{-2}$. The mean and
285 the median are 20.862 and 11.615 W m $^{-2}$, respectively.

286 We stress here that the objective of this study was not to provide an interpretation of this specific dataset, but rather
287 to increase the number of photosynthesis parameters available for usage in primary production models. A comprehensive
288 interpretation of the estimated parameter values would necessitate a detailed oceanographic analysis and knowledge
289 of regional, or local biogeochemical processes, which falls outside the scope of the present work and is a potential
290 course for future research. To facilitate this, we provide the obtained parameter values in a table published online at
291 <https://zenodo.org/records/17973417> (Kovač et al., 2025). Along with each estimated pair of photosynthesis parameters
292 we provide the original profile number given by Mattei & Scardi (2021) so that the parameter values can be traced back
293 to the profiles from which they had been estimated. We also give the date of each profile, along with coordinates. To
294 be more precise the data are comprised of the following: date (year, month, day), latitude, longitude, initial slope α^B ,
295 assimilation number P_m^B and the original profile number from Mattei & Scardi (2021), each given in a separate column.
296 There are also instances where one parameter value is estimated, but the other is not, due to insufficient information in
297 the measured primary production profiles to reliably estimate both parameters. Therefore, we only published parameter
298 pairs in which values of both parameters were estimated successfully, in line with the limitations set by the experiment
299 and the inverse procedure, described in detail in Kovač et al. (2016b). We also flag the values where the inverse procedure
300 did not result in realistic values of photosynthesis parameters with 0, the ones where the initial slope is too high with 0.5

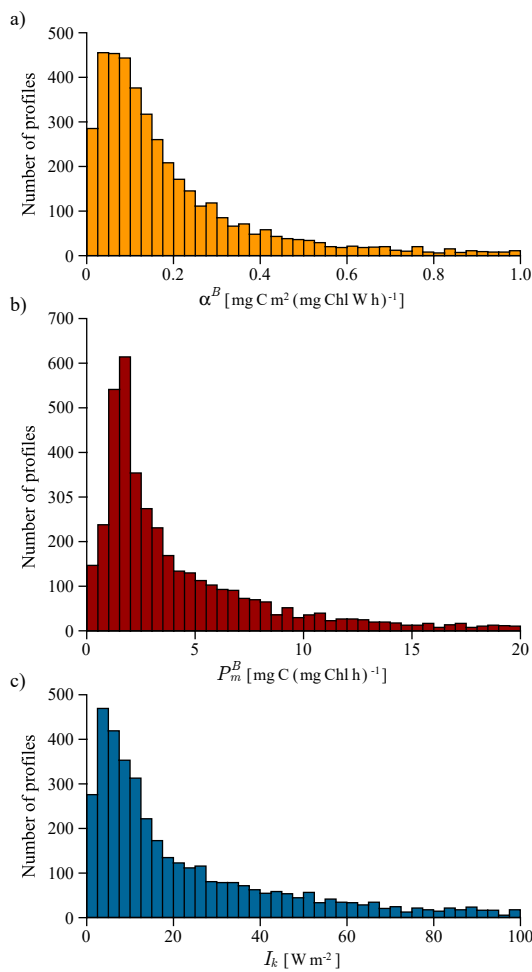


Figure 5: Histograms of the estimated photosynthesis parameters: a) Distribution of the initial slope α^B , b) Distribution of the assimilation number P_m^B , c) Photoadaptation parameter I_k . The horizontal axis shows parameter values, and the vertical axis indicates the percentage of profiles within each interval of those values.

301 and the realistic values with 1.

302 In the provided table, parameter values for which the inverse model did not converge onto realistic values are flagged
 303 and given as NaN. In some of these cases the model did yield reasonable estimates for watercolumn production, but for
 304 unrealistic values of photosynthesis parameters. This occurs due to the fact that watercolumn production is not uniquely
 305 determined by the photosynthesis parameters, but the production profile is (Kovač et al., 2016b). Therefore, the method
 306 may converge on a combination of parameter values for which watercolumn production is estimated rather well, but the
 307 production profile is not. In short, for those cases, the model gives the correct answer for watercolumn production, but
 308 for the wrong reasons. Keeping in mind the parameter values are estimated from the shape of the production profile we
 309 consider the error in the profile to take precedence. Another reason for plausible divergence in the values of photosynthesis
 310 parameters is the potential lack of information in the shape of the production profile to estimate both parameters. Under
 311 certain irradiance conditions, and based on the optical depths at which the incubations have been carried out, there may
 312 only be sufficient information on one parameter to be estimated (Kovač et al., 2016b). If this is the case, the value of the
 313 other parameter is not uniquely determined by the measured production profile and the inverse model estimate of that

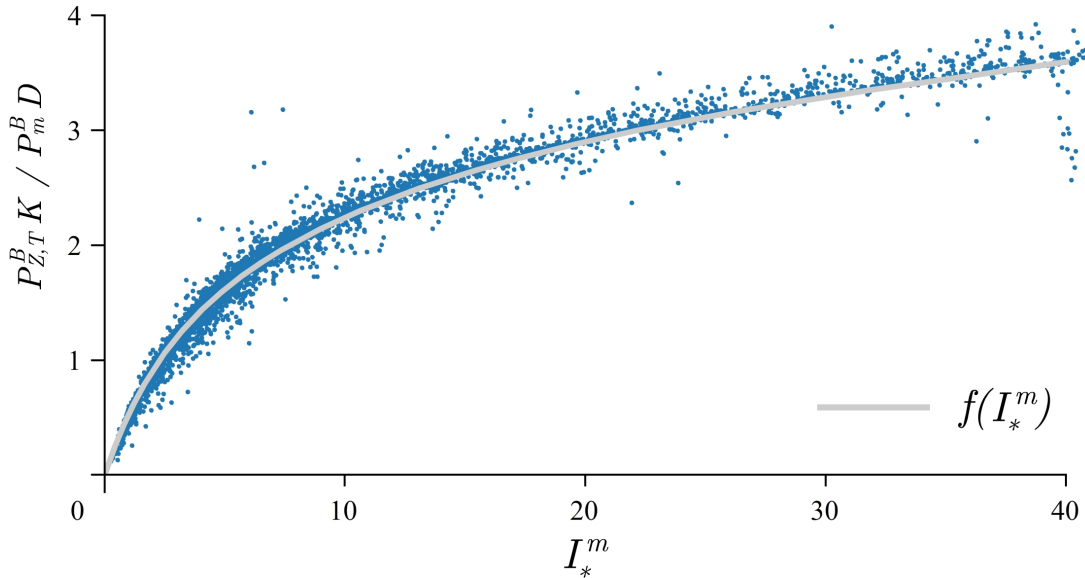


Figure 6: Comparison of measured normalized watercolumn production versus the analytical solution for normalized daily watercolumn production (18) by Platt et al. (1990). The abscissa represents the dimensionless noon irradiance I_*^m (19) while the ordinate gives the normalized watercolumn production divided by $P_m^B D / K$. The solid curve corresponds to the $f(I_*^m)$ function.

314 parameter value can diverge. In such instances the parameter values were also flagged.

315 The estimated photosynthesis parameters allows us to further calculate model accuracy, which to the best of our
 316 knowledge has not been done thus far on such a large in situ dataset. Model accuracy can be tested on production at
 317 depth as well as on watercolumn production. Of primary interest in remote sensing applications would be the latter,
 318 whereas for parameter estimation the former is of higher importance. Before presenting model accuracy, we should
 319 highlight that similar analysis have been performed by Behrenfeld & Falkowski (1997b) on the Ocean productivity
 320 dataset, which at the time of publication in 1997 had 10857 individual incubations (their Figure 4). That dataset is
 321 now a subset of the Mattei & Scardi (2021) dataset, which holds 37723 individual incubations, whilst keeping most of
 322 the Behrenfeld & Falkowski (1997b) data within it. The details on which data from Behrenfeld & Falkowski (1997b) are
 323 included in the the Mattei & Scardi (2021) dataset is provided in their paper.

324 To present the overall model fitness in calculating watercolumn production, we use the estimated parameter values
 325 to normalize the data and compare it to the Platt et al. (1990) analytical solution for watercolumn production, following
 326 the procedure described in Kovač et al. (2016a). For the Platt et al. (1980) photosynthesis irradiance function, used in
 327 this work, exact analytical solution for normalized watercolumn production can be written as:

$$P_{Z,T}^B = \frac{P_m^B D}{K} f(I_*^m), \quad (18)$$

328 where:

$$I_*^m = \frac{\alpha^B I_0^m}{P_m^B}, \quad (19)$$

329 is the normalized noon irradiance and $f(I_*^m)$ a known function (see Appendix A). By rewriting the above expression as:

$$\frac{K P_{Z,T}^B}{P_m^B D} = f\left(\frac{\alpha^B I_0^m}{P_m^B}\right), \quad (20)$$

330 and using the estimated parameter values $\hat{\alpha}^B$ and \hat{P}_m^B , along with noon irradiance \tilde{I}_0^m , enables the calculation of I_*^m ,
 331 which is the argument of the f function on the right hand side. On the left hand side, daylength D is known for each

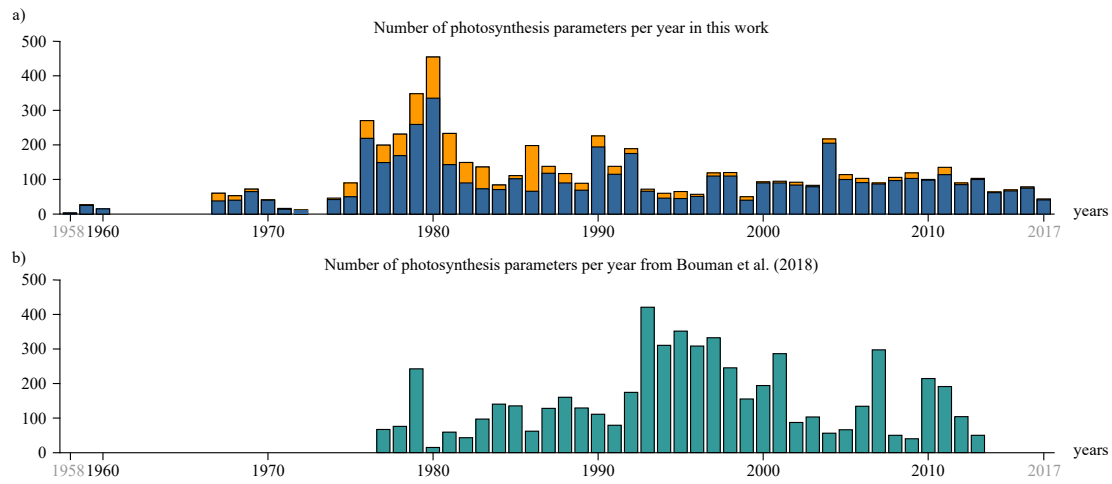


Figure 7: Time series of the global number of publicly available photosynthesis parameters. a) Parameter values estimated from in situ production profiles under natural light conditions estimated in this work. In blue is the number of successfully estimated photosynthesis parameters, whereas in orange is the number of available production profiles (same as in Figure 4.d). b) Parameter values estimated from in vitro experiments under controlled light conditions, published by Bouman et al. (2018), given in green.

measured profile and the attenuation coefficient is measured \tilde{K} . From the measured normalised production profile $\tilde{P}_T^B(z_n)$ (7), normalised watercolumn production is easily calculated using the trapezoidal rule. Therefore, the left hand side is known. This further enables the comparison of the $f(I_*^m)$ function with the entire dataset, by simply plotting the data as ordered pairs $(\hat{\alpha}^B \tilde{I}_0^m / \hat{P}_m^B, \tilde{K} \tilde{P}_{Z,T}^B / \hat{P}_m^B D)$ on the same plot as $f(I_*^m)$. Details on this procedure are provided in Kovač et al. (2016a). The results are given in Figure 6. The coefficient of determination R^2 of our model is 71.31 %.

In comparison to Kovač et al. (2016a) the optimal function used here (10) has the additional constraint on normalised watercolumn production. This helps the inverse model to come close to the measured estimate of normalised watercolumn production, while simultaneously describing the production profile. Upon testing the inverse model we have found this to be advantageous, as it prevents it from diverging in numerous cases. It also aided in constraining the estimate of watercolumn production, by balancing the estimate of production at depth alongside watercolumn production. The benefit from simultaneously constraining watercolumn production and production at all measured depths was most pronounced with profiles having a small number of measurement depths.

5 Discussion

In contemporary oceanography, estimation of global primary production is carried out using remote sensing algorithms (Westberry et al., 2023) and biogeochemical models (Follows et al., 2007). In both, primary production is calculated using parameters that describe the response of phytoplankton photosynthesis to available light. This response is described mathematically using photosynthesis irradiance functions (Platt & Jassby, 1976; Jones et al., 2014). These functions are uniquely determined by two parameters: the initial slope and the assimilation number, together termed the photosynthesis parameters (Sakshaug et al., 1997). Unlike other essential parameters and variables that are used in primary production models, such as chlorophyll, attenuation coefficient and photosynthetically available radiation, photosynthesis parameters are unfortunately not easily amenable to remote sensing, making photosynthesis parameter assignment a bottleneck in global primary production models. Given that global calculations of primary production are very sensitive to photosynthesis parameters (Platt et al., 1988; Kulk et al., 2020, 2021) and given we cannot regularly estimate them by



355 remote sensing, the increase in spatio-temporal coverage in photosynthesis parameters becomes a priority. In line with
356 this, active research on photosynthesis irradiance functions and novel methods for parameter estimation, with the aim of
357 refining models and increasing the availability of photosynthesis parameters, is still ongoing (Amirian et al., 2025; Britten
358 et al., 2025).

359 One of the approaches to the assignment of parameters has been on the basis of ecological provinces, following the
360 pioneering work of Longhurst et al. (1995). To implement, large amounts of field data were, and still are, required
361 (Platt et al., 2008). These data typically include chlorophyll, primary production, surface irradiance and the attenuation
362 coefficient. Ideally, photosynthesis irradiance experiments are performed in as many locations and seasons as possible,
363 and archived (Platt et al., 2017). Having photosynthesis parameters at our disposal then enables coupling of the in situ
364 data to the remotely sensed data via various algorithmic approaches (Platt et al., 2008; Picart et al., 2014). This then
365 makes possible the inverse, which is the assignment of photosynthesis parameters to a given region of the ocean (Platt &
366 Sathyendranath, 1999; Devred et al., 2007).

367 Photosynthesis irradiance experiments have been carried out numerous times yielding parameters in various oceans
368 and seas, with the most recent published global archive of photosynthesis parameters by Bouman et al. (2018) containing
369 5711 parameter values globally. Most of the Bouman et al. (2018) data are from the North Atlantic and the Arctic, with
370 pockets of data in the Southern Ocean, Indian Ocean and in the South Atlantic, with scarcely any data in the Pacific
371 ocean (Figure 3), such that the global ocean is spatially undersampled with respect to photosynthesis parameters.

372 The photosynthesis parameters estimated from the Mattei & Scardi (2021) dataset complement the direct estimates
373 with respect to location (Figure 3), filling gaps in many parts of the world ocean. The dataset contains 6084 measured
374 production profiles from the global oceans. It is comprised of already published and freely available data, as well as
375 some data which were less well known. By using the inverse model (Kovač et al., 2016a,b) we were able to estimate 3776
376 photosynthesis parameters pairs from this dataset and thereby we have created a new dataset containing photosynthesis
377 parameters from the North Pacific Ocean, the Eastern Equatorial Pacific Ocean, close to both the east and west coasts
378 of North America, the Indian Ocean and the northern high latitudes (Figure 3). A large swath of the Eastern Pacific
379 Ocean in the equatorial region is also covered. In comparison to the Bouman et al. (2018) dataset, also shown in Figure
380 3, the new dataset complements and increases the spatial coverage of photosynthesis parameters in the global ocean. In
381 both the Bouman et al. (2018) and the new dataset, there are also scattered pockets of data from various other regions
382 of the ocean.

383 From the temporal standpoint these datasets are not by any means homogenous in the number of parameters per
384 year (Figure 7). The number per year is low, both for the new dataset developed here, and for the Bouman et al. (2018)
385 dataset. The Bouman et al. (2018) dataset begins in 1977 and ends in 2013, whereas the new one starts in 1960 and ends in
386 2017. Construction of a joint time series using both datasets would not be a trivial problem, because of the disparities in
387 time and location. Nevertheless, construction of local time series of photosynthesis parameters would be plausible, given
388 there are time series stations at which photosynthesis parameters have been estimated from in situ production profiles.
389 For example, at the Hawaii Ocean Time Series and the Bermuda Atlantic Time Series, photosynthesis parameters have
390 been estimated by Kovač et al. (2016a) and Kovač et al. (2018), respectively. Some of those data are also contained in
391 the Mattei & Scardi (2021) dataset. Primary production measurements are ongoing at those stations, though the latest
392 values are not, naturally, included in the Mattei & Scardi (2021) dataset. Measurements at Hawaii Ocean Time Series
393 started in 1989 and at Bermuda Atlantic Time Series in 1988. Therefore, there is a potential to construct time series
394 of photosynthesis parameters that are at least 30 years long at these locations. The construction of such time series
395 would provide testing grounds for studying the effect of time dependent photosynthesis parameters on remote sensing
396 algorithms and ecosystem models. This might improve the current estimates at these time series (Wu et al., 2024) and



397 assist in future modelling efforts (Zheng et al., 2025).

398 Time series analysis of the photosynthesis parameters themselves would also help assess whether seasonal variability
399 in photosynthesis parameters dominates over the interannual variability, or vice versa, and to study the rate of change
400 of photosynthesis parameters. Information on the time scales of variability would help mold future developments in
401 remote sensing algorithms and help in parameter assignment procedures more broadly, like in marine ecosystem models.
402 Naturally, analysis of trends would be possible once such time series had been established. These are all potential
403 applications of the dataset assembled here.

404 In this context, the importance of proper data storage and accessibility, cannot be exaggerated. This work would not
405 have been possible without the publicly available dataset from Mattei & Scardi (2021). From the historical standpoint,
406 production profiles data are not distributed under a central data hub and subsequently are not easily accessible. From
407 the standpoint of primary production models, this is unfortunate, as quality data are essential for model development
408 and testing, arguably with a minimum standard for archiving data satisfied (Platt et al., 2017). When measuring primary
409 production at sea, the essential variables that are typically archived are the chlorophyll and primary production profiles.
410 These should be complemented by archiving daily irradiance and the irradiance profile ideally, whenever available. Having
411 such auxiliary information would allow the estimation of photosynthesis parameters, as demonstrated here. If, however,
412 information on surface and underwater irradiance is not stored, statistical methods, such as Bayesian approaches or
413 machine learning algorithms, could be used for estimating photosynthesis parameters. Such methods could also provide
414 reliable uncertainty measures for photosynthesis parameters and potentially also for watercolumn production estimates.
415 They might also be able to relax the requirement on the minimum number of vertical levels at which the production profiles
416 have to be measured. Therefore, we recognize the application of Bayesian methods and machine learning algorithms are
417 a potential course for future research.

418 A point that merits consideration is whether the parameters extracted from in situ primary production data subjected
419 to inverse modelling techniques applied to a non-spectral model, as is done here, would be directly applicable to a spectral
420 model of primary production. It has been demonstrated (Sathyendranath & Platt, 2007) that spectral models and non-
421 spectral models of primary production are fundamentally different from each other in one major respect: spectral models
422 are able to account for the spectral variability in underwater light fields, and for the covariance of spectrally-resolved
423 light with the spectral variability in the action spectrum of photosynthesis. Here, action spectrum is the term used to
424 describe the spectral variability in α^B . Direct measurements of action spectrum in the field are rare (but see Lewis et al.
425 (1985), Schofield et al. (1991), Kyewalyanga et al. (1997)); and so spectral models of primary production exploit the
426 similarity in the shape of the action spectrum with that of phytoplankton absorption (Kyewalyanga et al., 1998), but
427 allow the mean magnitude of the action spectrum to match the value of α^B measured under spectrally-neutral white light
428 (Sathyendranath & Platt, 1989a). It is therefore important that the α^B values provided as inputs to spectral models are
429 estimated under white light, or corrected for the spectral quality of light in the incubator. The α^B inferred from in situ
430 primary-production profile, on the other hand, correspond to the spectral quality of the light that the phytoplankton
431 experienced at the time of their incubations. Therefore, α^B inferred using a non-spectral model should not be used
432 without appropriate correction to a spectral model.

433 Spectral quality of light becomes important when combining in situ experiments with simulated in situ incubations.
434 In the latter, the samples are incubated on deck (rather than under water), and different filters are used to reduce the
435 light level reaching the samples to simulate light levels reaching different depths of the water column. Often, these are
436 neutral filters such that there is no attempt to simulate the spectral quality of light underwater. On the other hand, in
437 some experiments, green or blue filters are used to represent better the spectral quality of light underwater. The Mattei
438 and Scardi (2021) database contains data from in situ incubations and simulated in situ incubations. They have all been



439 treated alike in the inverse model, and hence are subject to some unknown uncertainties associated with the spectral
440 quality of light in the simulated in situ experiments.

441 In addition to this, most ocean colour models estimate primary production on a daily timescale, which aligns with both
442 the approximate duration of phytoplankton cell division and the temporal resolution at which phytoplankton biomass
443 can be observed using Earth-orbiting satellites (Marra, 2002). However, rate parameters derived from conventional short-
444 term (2 to 3 hours) photosynthesis irradiance incubations have been shown to exhibit diel periodicity (MacCaull & Platt,
445 1977; Prezelin et al., 1986; Harding et al., 1983; Bruyant et al., 2005). Such fluctuations in photosynthesis parameters are
446 not accounted for in current primary production models, which typically assume that photosynthesis parameters remain
447 constant throughout the day based on the assumption that diel variability is relatively minor compared to differences
448 observed across biogeochemical provinces (Babin et al., 1996). It has also been argued that respiratory losses relative to
449 carbon assimilation may also vary over the course of the day, which would also cause rates of carbon uptake to be dependent
450 on the duration of the incubation (Marra, 2009). This new dataset will allow future comparisons of photosynthesis
451 parameters derived from 24 hour in situ incubations with those derived from short-term photo-physiological experiments
452 (e.g. Bouman et al. (2018)) and will allow us to assess whether the two approaches yield similar spatio-temporal patterns
453 in photosynthetic response across a range of biogeochemical domains.

454 6 Conclusions

455 In this work we have derived a global set of photosynthesis parameters estimated from primary production profiles
456 published by Mattei & Scardi (2021). In the parameter estimation procedure we have used an analytically solvable model
457 of the production profile by Kovač et al. (2016a) as the forward model (Figure 1). For the inverse model we have used
458 an optimization procedure with the Nelder & Mead (1965) search algorithm, constrained by the analytical solution for
459 watercolumn production by Platt et al. (1990). We have discussed the advantages, as well as the limitations of the
460 approach stemming from both the model and the data (Figures 2 and 4). The overall model versus data comparison was
461 performed on watercolumn production, as shown in Figure 6, with the model performance being quite good, having an
462 R^2 of 71.31 %.

463 The new dataset of photosynthesis parameters that was constructed in this work is complementary to the prior dataset
464 published by Bouman et al. (2018) and provides a comparable spatio-temporal coverage (Figures 3 and 7). With this
465 work the global archive of publicly available data on photosynthesis parameters has effectively doubled. A straightforward
466 application of the new photosynthesis parameters dataset is in global primary production models, such as by Kulk et al.
467 (2020, 2021), or in biogeochemical models, such as by Follows et al. (2007). The new dataset is publicly available at
468 <https://zenodo.org/records/17973417> (Kovač et al., 2025), along with metadata for referencing it to the original Mattei
469 & Scardi (2021) dataset.

470 Having the new dataset available opens the avenue for novel research directions, such as testing existing remote
471 sensing models with the novel parameter values in regions of the ocean where non where known prior, constructing
472 local or regional algorithms for photosynthesis parameters assignment, or constructing time series of photosynthesis
473 parameters. Also, having demonstrated that the recovery of photosynthesis parameters from such a large global dataset
474 is plausible, the application of other methods and models, might as well be a potential course for future research. From
475 an operational standpoint, we conclude that creating a global hub for primary production data, be it production profiles,
476 or photosynthesis irradiance experiments, is due.



477 7 Acknowledgments

478 This work was supported by the Croatian Science Foundation under the project number IP-2022-10-8859. This work was
 479 supported by the Simons Collaboration on Computational Biogeochemical Modeling of Marine Ecosystems/ CBIOMES
 480 (549947 to S.S.). We thank the authors Mattei & Scardi (2021) for the effort of collecting a global dataset of chlorophyll
 481 and primary production profiles. Without their prior work, this work would not have been possible. We also acknowledge
 482 the numerous scientists and ship staff that have been involved on all the cruises that were undertaken to gather this large
 483 dataset.

484 8 Data availability

485 The dataset of photosynthesis parameters created in this work is published in the Zenodo repository and is made publicly
 486 available (Kovač et al., 2025). It can be accessed via the following url: <https://zenodo.org/records/17973417>.

487 9 Author contributions

488 ŽK had the original idea. LĆ and ŽK did the initial data analysis. ŽK and MBK applied the inverse model. MBK did
 489 in depth analysis of the results. ŽK wrote the draft. MBK, SS, HB, GK and LĆ corrected the draft and wrote subsets
 490 of the manuscript. LĆ published the data on PANGEA. All authors discussed the results and contributed to the final
 491 manuscript.

492 Appendix A: Forward model

493 The primary production model used in this paper is based on the work of Platt et al. (1990) in which the exponential
 494 photosynthesis irradiance function from a previous paper, also by Platt et al. (1980), is used in (1):

$$495 p^B(I) = P_m^B (1 - \exp(-\alpha^B I / P_m^B)). \quad (21)$$

496 The underwater irradiance model is as stated in (3). Platt et al. (1990) have solved the watercolumn production integral
 497 (5) exactly for the case of uniform time independent biomass $B(z, t) = B$. Their solution reads:

$$498 P_{Z,T} = \frac{BP_m^B D}{K} f(I_*^m), \quad (22)$$

499 where the $f(I_*^m)$ function is given as:

$$500 f(I_*^m e^{-Kz}) = \sum_{n=1}^{\infty} \frac{2 (I_*^m e^{-Kz})^{2n-1}}{\pi (2n-1) (2n-1)!} \frac{(2n-2)!!}{(2n-1)!!} \\ - \sum_{n=1}^{\infty} \frac{(I_*^m e^{-Kz})^{2n}}{2n (2n)!} \frac{(2n-1)!!}{(2n)!!}. \quad (23)$$

501 By rearranging expression (22) the analytical solution for normalised watercolumn production (18) is obtained:

$$502 P_{Z,T}^B = \frac{P_m^B D}{K} f(I_*^m). \quad (24)$$

503 Based on the solution (24), in a paper by Kovač et al. (2016a), the analytical solution of the integral for the normalised
 504 daily production profile (4) was solved. It reads:

$$505 P_T^B(z) = P_m^B D f_z(I_*^m e^{-Kz}), \quad (25)$$



501 where now the $f_z(I_*^m e^{-Kz})$ function is given as:

$$f_z(I_*^m e^{-Kz}) = \sum_{n=1}^{\infty} \frac{2(I_*^m e^{-Kz})^{2n-1}}{\pi(2n-1)!} \frac{(2n-2)!!}{(2n-1)!!} \\ - \sum_{n=1}^{\infty} \frac{(I_*^m e^{-Kz})^{2n}}{(2n)!} \frac{(2n-1)!!}{(2n)!!}. \quad (26)$$

502 The two functions, (23) and (26), are related by:

$$f_z(I_*^m e^{-Kz}) = -\frac{1}{K} \frac{d}{dz} f(I_*^m e^{-Kz}). \quad (27)$$

503 From (25) the daily production profile is simply calculated by multiplication with biomass:

$$P_T = B(z) P_m^B D f_z(I_*^m e^{-Kz}), \quad (28)$$

504 where $B(z)$ is prescribed. The normalised daily production profile (25) and the normalised daily watercolumn production
 505 are then used in the optimal function of the inverse model (10) to estimate photosynthesis parameters from a measured
 506 normalised daily production profile.

507 Appendix B: Inverse model

508 For an individual survey, we have at disposal the following set of measurements: noon irradiance \tilde{I}_0^m , attenuation coefficient
 509 \tilde{K} , daylength \tilde{D} , production profile $\tilde{P}_T(z_n)$ and biomass profile $\tilde{B}(z_n)$, where $n = 1, 2, \dots, N$. By calculating the measured
 510 normalised production profile as:

$$\tilde{P}_T^B(z_n) = \tilde{P}_T(z_n) / \tilde{B}(z_n) \quad (29)$$

511 we formulate the error of the forward model as:

$$\mathcal{P}(\alpha^B, P_m^B) = \sum_{n=1}^N \left(P_m^B \tilde{D} f_z \left(\alpha^B \tilde{I}_0^m e^{-\tilde{K} z_n} / P_m^B \right) - \tilde{P}_T^B(z_n) \right)^2 \\ + \left(\frac{P_m^B \tilde{D}}{\tilde{K}} f(\alpha^B \tilde{I}_0^m / P_m^B) - \sum_{n=1}^N \tilde{P}_T^B(z_n) \Delta z_n \right)^2, \quad (30)$$

512 This function is then used as the optimal function in the inverse model. The first sum in the optimal function goes over
 513 the measurement depths and compares the model prediction $P_T^B(z_n | \alpha^B, P_m^B)$ with the measured value at that depth
 514 $\tilde{P}_T^B(z_n)$ (green dots on the right in Figure 1). The second term compares the model prediction of normalised watercolumn
 515 production $P_m^B \tilde{D} f(\alpha^B \tilde{I}_0^m / P_m^B) / \tilde{K}$ with the measured normalised daily watercolumn production $\sum_{n=1}^N \tilde{P}_T^B(z_n) \Delta z_n$ (blue
 516 surface on the right in Figure 1). The photosynthesis parameter values at the minimum of $\mathcal{P}(\alpha^B, P_m^B)$ are taken as the
 517 optimal values and are labelled as: $\hat{\alpha}^B$ and \hat{P}_m^B .

518 In the implementation stage of the inverse model we have opted to use the Nelder-Mead optimization algorithm
 519 (Nelder & Mead, 1965), a direct search algorithm already tested on this type of problems by Kovač et al. (2016a,b). To
 520 reduce the search in the parameter space we have set the constraints on the photosynthesis parameters to be positive,
 521 namely $\alpha^B > 0$ and $P_m^B > 0$, given that by definition the parameters are positive. Also, the two analytical expressions
 522 used in the optimal function (30), one for the normalised daily production profile and the other for the normalised daily
 523 watercolumn production, are both infinite sums. This implies that at implementation these sums have to be truncated
 524 and we have opted to truncate both at 50 elements in the sum.

525 Bibliography

526 Amirian, M. M., Finkel, Z. V., Devred, E., & Irwin, A. J. (2025). Parameterization of photoinhibition for phytoplankton. *Communications
 527 Earth and Environment*, 6:707, 1–9. doi:10.1038/s43247-025-02686-3.



528 Antoine, D., Andre, J. M., & Morel, A. (1996). Oceanic primary production. 2. estimation at global scale from satellite (coastal zone color
529 scanner) chlorophyll. *Global Biogeochemical Cycles*, 10, 57–69. doi:10.1029/95GB02832.

530 Babin, M., Morel, A., Claustre, H., Bricaud, A., Kolber, Z., & Falkowski, P. J. (1996). Nitrogen- and irradiance-dependent variations of
531 the maximum quantum yield of carbon fixation in eutrophic, mesotrophic and oligotrophic marine systems. *Deep-Sea Research I*, 43(8),
532 1241–1272.

533 Balch, W., Evans, R., Brown, J., Feldman, G., McClain, C., & Esalas, W. (1992). The remote sensing of ocean primary productivity: Use of
534 a new data compilation to test satellite algorithms. *Journal of Geophysical Research*, 97(2), 2279–2293. doi:10.1029/91JC02843.

535 Behrenfeld, M. J., & Falkowski, P. G. (1997a). A consumer's guide to phytoplankton primary productivity models. *Limnology and Oceanog-
536 raphy*, 42(7), 1479–1491. doi:10.4319/lo.1997.42.7.1479.

537 Behrenfeld, M. J., & Falkowski, P. G. (1997b). Photosynthetic rates derived from satellite-based chlorophyll concentration. *Limnology and
538 Oceanography*, 42, 1–20. doi:10.4319/lo.1997.42.1.0001.

539 Behrenfeld, M. J., Prasil, O., Babin, M., & Bruylants, F. (2004). In search of a physiological basis for covariations in light-limited and
540 light-saturated photosynthesis. *Journal of Phycology*, 40, 4–25. doi:10.1046/j.1529-8817.2004.03083.x.

541 Bouman, H. A., Platt, T., Dobbin, M., Figueiras, F. G., Gudmundsson, K., Gudfinnsson, H. G., Huang, B., Hickman, A., Hiscock, M.,
542 Jackson, T., Lutz, V. A., Mélin, F., Rey, F., Pepin, P., Segura, V., Tilstone, G. H., van Dongen-Vogels, V., & Sathyendranath, S. (2018).
543 Photosynthesis-irradiance parameters of marine phytoplankton: synthesis of a global data set. *Earth System Science Data*, 10, 251–266.
544 doi:10.5194/essd-10-251-2018.

545 Brewin, R., Sathyendranath, S., Kulk, G., Rio, M.-H., Concha, J., Bell, T., Bracher, A., Fichot, C., Frölicher, T., Gallo, M., Hansell, D.,
546 Kostadinov, T., Mitchell, C., Neeley, A., Organelli, E., Richardson, K., Rousseaux, C., Shen, F., Stramski, D., Tzortziou, M., Watson,
547 A., Addey, C., Bellacicco, M., Bouman, H., Carroll, D., Cetinić, I., Dall'Olmo, G., Frouin, R., Hauck, J., Hieronymi, M., Hu, C., Ibello,
548 V., Jönsson, B., Kong, C., Kovač, J., Laine, M., Lauderdale, J., Lavender, S., Livanou, E., Llort, J., Lorinczi, L., Nowicki, M., Pradist, Y.,
549 N., Psarra, S., Raitos, D., Ruescas, A., Russell, J., Salisbury, J., Sanders, R., Shutler, J., Sun, X., Taboada, F., Tilstone, G., Wei, X.,
550 & Woolf, D. (2023). Ocean carbon from space: Current status and priorities for the next decade. *Earth-Science Reviews*, 240, 104386.
551 doi:10.1016/j.earscirev.2023.104386.

552 Britten, G. L., Jonsson, B., Kul, G., Bouman, H. A., Follows, M. J., & Sathyendranath, S. (2025). Predicting
553 photosynthesis-irradiance relationships from satellite remote-sensing observations. *Limnology and Oceanography Letters (accepted)*, .
554 doi:10.22541/essoar.172588647.73876296/v1.

555 Bruylants, F., Babin, M., Genty, B., Prasil, O., Berhrenfeld, M. J., Claustre, H., Bricaud, A., Garczarek, L., Holtzendorff, J., Koblizek, M.,
556 Dousova, H., & Partensky, F. (2005). Diel variations in the photosynthetic parameters of prochlorococcus strain pcc 9511: combined effects
557 of light and cell cycle. *Limnology and Oceanography*, 50, 850–863. doi:10.4319/lo.2005.50.3.0850.

558 Buitenhuis, E. T., Hashioka, T., & Quéré, L. (2013). Combined constraints on global ocean primary production using observations and models.
559 *Global Biogeochemical Cycles*, 27, 847–858. doi:10.1002/gbc.20074.

560 Campbell, J., Antoine, D., Armstrong, R., Arrigo, K., Balch, W., Barber, R., Behrenfeld, M. J., Bidigare, R., Bishop, J., Carr, M., & et. al.
561 (2002). Comparison of algorithms for estimating ocean primary production from surface chlorophyll, temperature, and irradiance. *Global
562 biogeochemical cycles*, 16, 9–15. doi:10.1029/2001GB001444.

563 Devred, E., Sathyendranath, S., & Platt, T. (2007). Delineation of ecological provinces using ocean colour radiometry. *Marine Ecology Progress
564 Series*, 346, 1–13. doi:10.3354/meps07149.

565 Falkowski, P. G. (1981). Light-shade adaptation and assimilation numbers. *Journal of Plankton Research*, 3, 203–216.
566 doi:10.1093/plankt/3.2.203.

567 Follows, M. J., Dutkiewicz, S., Grant, S., & Chisholm, S. W. (2007). Emergent biogeography of microbial communities in a model ocean.
568 *Science*, 315, 1843–1846. doi:10.1126/science.1138544.

569 Frenette, J., Demers, S., & Legendre, L. (1993). Lack of agreement among models for estimating the photosynthetic parameters. *Limnology
570 and Oceanography*, 38, 679–687. doi:10.4319/lo.1993.38.3.0679.



571 Friedlingstein, P., O'Sullivan, M., Jones, M. W., Andrew, R. M., Hauck, J., Landschützer, P., Le Quéré, C., Li, H., Luijkx, I. T., Olsen, A.,
572 Peters, G. P., Peters, W., Pongratz, J., Schwingshackerl, C., Sitch, S., Canadell, J. G., Ciais, P., Jackson, R. B., Alin, S. R., Arneth, A.,
573 Arora, V., Bates, N. R., Becker, M., Bellouin, N., Berghoff, C. F., Bittig, H. C., Bopp, L., Cadule, P., Campbell, K., Chamberlain, M. A.,
574 Chandra, N., Chevallier, F., Chini, L. P., Colligan, T., Decayeux, J., Djeutchouang, L. M., Dou, X., Duran Rojas, C., Enyo, K., Evans,
575 W., Fay, A. R., Feely, R. A., Ford, D. J., Foster, A., Gasser, T., Gehlen, M., Gkrizalis, T., Grassi, G., Gregor, L., Gruber, N., Gürses, ,
576 Harris, I., Hefner, M., Heinke, J., Hurtt, G. C., Iida, Y., Ilyina, T., Jacobson, A. R., Jain, A. K., Jarníková, T., Jersild, A., Jiang, F., Jin,
577 Z., Kato, E., Keeling, R. F., Klein Goldewijk, K., Knauer, J., Korsbakken, J. I., Lan, X., Lauvset, S. K., Lefèvre, N., Liu, Z., Liu, J., Ma,
578 L., Maksyutov, S., Marland, G., Mayot, N., McGuire, P. C., Metzl, N., Monacci, N. M., Morgan, E. J., Nakaoaka, S.-I., Neill, C., Niwa, Y.,
579 Nützel, T., Olivier, L., Ono, T., Palmer, P. I., Pierrot, D., Qin, Z., Resplandy, L., Roobaert, A., Rosan, T. M., Rödenbeck, C., Schwinger,
580 J., Smallman, T. L., Smith, S. M., Sospedra-Alfonso, R., Steinhoff, T. et al. (2024). Global carbon budget 2024. *Earth System Science
Data*, 17(3), 965–1039. doi:10.5194/essd-17-965-2025.

582 Gallegos, C. L., & Platt, T. (1981). Photosynthesis measurements on natural populations of phytoplankton: Numerical analysis. In *Physiological
bases of phytoplankton ecology* (pp. 103–112). Canadian bulletin of fisheries and aquatic sciences.

584 Gordon, H. R., Wang, M., Brown, J. W., Brown, O. B., Evans, R. H., & Broenkow, W. W. (1983). Phytoplankton pigment concentrations in
585 the middle atlantic bight: comparison of ship determinations and czcs estimates. *Applied Optics*, 22(1), 20–36. doi:10.1364/ao.22.000020.

586 Harding, L. W., Meeson, B. W., & Tyler, M. A. (1983). Photoadaptation and diel periodicity of photosynthesis in the dinoflagellate pror-
587 centrum mariaeaebouriae. *Marine Ecology Progress Series*, 13, 73–85. doi:10.3354/meps013073.

588 Jassby, A. D., & Platt, T. (1976). Mathematical formulation of the relationship between photosynthesis and light for phytoplankton. *Limnology
and Oceanography*, 21, 540–547. doi:10.4319/lo.1976.21.4.0540.

590 Jones, C. T., Craig, S. E., Barnett, A. B., MacIntyre, H. L., & Cullen, J. J. (2014). Curvature in models of the photosynthesis-irradiance
591 response. *Journal of Phycology*, 50, 341–355. doi:10.1111/jpy.12164.

592 Kirk, J. T. O. (2011). *Light and photosynthesis in aquatic ecosystems*. (3rd ed.). Cambridge University Press. doi:10.1017/CBO9780511623370.

593 Kovač, Z., Baćeković Koloper, M., Sathyendranath, S., Kulk, G., Bouman, H., & Ćatićović, L. (2025). Global marine photosynthesis parameters
594 dataset [data set]. *Zenodo*, . doi:https://doi.org/10.5281/zenodo.17973417.

595 Kovač, Z., Platt, T., Antunović, S., Sathyendranath, S., Morović, M., & Gallegos, C. (2017a). Extended formulations and analytic solutions
596 for watercolumn production integrals. *Frontiers in Marine Science*, 4:163. doi:10.3389/fmars.2017.00163.

597 Kovač, Z., Platt, T., S., S., & Antunović, S. (2017b). Models for estimating photosynthesis parameters from in situ production profiles.
598 *Progress in Oceanography*, 159, 255–266. doi:10.1016/j.pocean.2017.10.013.

599 Kovač, Z., Platt, T., Sathyendranath, S., & Lomas, M. W. (2018). Extraction of photosynthesis parameters from time series measurements of
600 in situ production: Bermuda atlantic time-series study. *Remote Sensing*, 10, 915. doi:10.3390/rs10060915.

601 Kovač, Z., Platt, T., Sathyendranath, S., & Morović, M. (2016a). Analytical solution for the vertical profile of daily production in the ocean.
602 *Journal of Geophysical Research: Oceans*, 121. doi:10.1002/2015JC011293.

603 Kovač, Z., Platt, T., Sathyendranath, S., Morović, M., & Jackson, T. (2016b). Recovery of photosynthesis parameters from *in situ* profiles of
604 phytoplankton production. *ICES Journal of Marine Science*, 73 (2), 275–285. doi:10.1093/icesjms/fsv204.

605 Kulk, G., Platt, T., Dingle, J., Jackson, T., Johnsson, B., Bouman, H. A., Doblin, M., Estrada, M., Figueiras, F. G., Furuya, K., Gonzalez, N.,
606 Huang, B., Isada, Z. L. V., T. Kovac, Maranon, E., Raman, M., Richardson, K., Rozema, P. D., van de Poll, W. H., Segura, V., Tilstone,
607 G. H., & Sathyendranath, S. (2020). Primary production, an index of climate change in the ocean: Satellite-based estimates over two
608 decades. *Remote Sensing*, 12 (5), 826. doi:10.3390/rs12050826.

609 Kulk, G., Platt, T., Dingle, J., Jackson, T., Johnsson, B., Bouman, H. A., Doblin, M., Estrada, M., Figueiras, F. G., Furuya, K., Gonzalez, N.,
610 Huang, B., Isada, Z. L. V., T. Kovac, Maranon, E., Raman, M., Richardson, K., Rozema, P. D., van de Poll, W. H., Segura, V., Tilstone,
611 G. H., & Sathyendranath, S. (2021). Correction: Primary production, an index of climate change in the ocean: Satellite-based estimates
612 over two decades. *Remote Sensing*, 13 (17), 3462. doi:10.3390/rs13173462.

613 Kyewalyanga, M., Platt, T., & Sathyendranath, S. (1992). Ocean primary production calculated by spectral and broad-band models. *Marine
614 Ecology Progress Series*, 85, 171–185. doi:10.3354/meps085171.



615 Kyewalyanga, M. N., Platt, T., & Sathyendranath, S. (1997). Estimation of the photosynthetic action spectrum: implication for primary
616 production models. *Marine Ecology Progress Series*, 146, 207–223. doi:10.3354/meps146207.

617 Kyewalyanga, M. N., Platt, T., & Sathyendranath, S. (1998). Seasonal variations in physiological parameters of phytoplankton across the
618 north atlantic. *Journal of Plankton Research*, 20(1), 17–42. doi:10.1093/plankt/20.1.17.

619 Lewis, M. R., Warnock, R. E., Irwin, B., & Platt, T. (1985). Measuring photosynthetic action spectra of natural phytoplankton populations.
620 *Journal of Phycology*, 21, 310–315. doi:10.1111/j.0022-3646.1985.00310.x.

621 Longhurst, A., Sathyendranath, S., & Platt, T. (1995). An estimate of global primary production in the ocean from satellite radiometer data.
622 *Journal of Plankton Research*, 17, 1245–1271. doi:10.1093/plankt/17.6.1245.

623 MacCaull, W. A., & Platt, T. (1977). Diel variations in the photosynthetic parameters of coastal marine phytoplankton. *Limnology and
624 Oceanography*, 22(4), 723–731. doi:10.4319/lo.1977.22.4.0723.

625 MacIntyre, H. L., Kana, T. M., Anning, T., & Geider, R. (2002). Photoacclimation of photosynthesis irradiance response curves and photo-
626 synthetic pigments in microalgae and cyanobacteria. *Journal of Phycology*, 38, 17–38. doi:10.1046/j.1529-8817.2002.00094.x.

627 Marra, J. (2002). Approaches to the measurements of plankton production. In *Phytoplankton productivity - Carbon assimilation in marine
628 and freshwater ecosystems* (pp. 78–108). Blackwell Science. doi:10.1002/9780470995204.

629 Marra, J. (2009). Net and gross productivity: weighing in with 14c. *Aquatic Microbial Ecology*, 56, 123–131. doi:10.3354/ame01306.

630 Marshall, H. L., Geider, R. J., & Flynn, K. J. (2000). A mechanistic model of photoinhibition. *New Phytologist*, 145, 347–359. doi:10.1046/j.1469-
631 8137.2000.00575.x.

632 Mattei, F., & Scardi, M. (2021). Collection and analysis of a global marine phytoplankton primary-production dataset. *Earth System Science
633 Data*, 13, 4967–4985. doi:10.5194/essd-13-4967-2021.

634 Milligan, A., Hasley, K. M., & Behrenfeld, M. J. (2015). Advancing interpretations of 14C-uptake measurements in the context of phytoplankton
635 physiology and ecology. *Journal of plankton research*, 37, 692–698. doi:10.1093/plankt/fbv051.

636 Morel, A., & Smith, R. C. (1974). Relation between total quanta and total energy for aquatic photosynthesis. *Limnology and Oceanography*,
637 19, 591–600. doi:10.4319/lo.1974.19.4.0591.

638 Nelder, J. A., & Mead, R. (1965). A simplex method for function minimization. *Computer Journal*, 7, 308–313. doi:10.1093/comjnl/7.4.308.

639 Peterson, B. J. (1980). Aquatic primary production and the 14C-CO₂ method: A history of the productivity problem. *Annual Review of
640 Ecology, Evolution and Systematics*, 11, 359–385.

641 Picart, S. S., Sathyendranath, S., Dowell, M., Moore, T., & Platt, T. (2014). Remote sensing of assimilation number for marine phytoplankton.
642 *Remote Sensing of Environment*, 146, 87–96. doi:10.1016/j.rse.2013.10.032.

643 Platt, T., Caverhill, C., & Sathyendranath, S. (1991). Basin-scale estimates of oceanic primary production by remote sensing: The North
644 Atlantic. *Journal of Geophysical Research*, 96, 15147–15159. doi:10.1029/91JC01118.

645 Platt, T., Denman, K. L., & Jassby, A. D. (1977). Modelling the productivity of phytoplankton. In *The sea: ideas and observations on
646 progress in the study of the seas* (pp. 807–856). Wiley, New York.

647 Platt, T., Gallegos, C. L., & Harrison, W. G. (1980). Photoinhibition of photosynthesis in natural assemblages of marine phytoplankton.
648 *Journal of Marine Research*, 38, 687–701.

649 Platt, T., & Jassby, A. (1976). The relationship between photosynthesis and light for natural assemblages of coastal marine phytoplankton.
650 *Journal of Phycology*, 12, 421–430. doi:10.1111/j.1529-8817.1976.tb02866.x.

651 Platt, T., & Sathyendranath, S. (1988). Oceanic primary production: Estimation by remote sensing at local and regional scales. *Science*, 241,
652 1613–1620. doi:10.1126/science.241.4873.1613.

653 Platt, T., & Sathyendranath, S. (1991). Biological production models as elements of coupled, atmosphere-ocean models for climate research.
654 *Journal of Geophysical Research*, 96, 2585–2592. doi:10.1029/90JC02305.

655 Platt, T., & Sathyendranath, S. (1993). Estimators of primary production for interpretation of remotely sensed data on ocean color. *Journal
656 of Geophysical Research*, 98, 14561–14576.



657 Platt, T., & Sathyendranath, S. (1999). Spatial structure of pelagic ecosystem processes in the global ocean. *Ecosystems*, *2*, 384–394.
658 doi:10.1007/s100219900088.

659 Platt, T., Sathyendranath, S., Caverhill, C. M., & Lewis, M. R. (1988). Ocean primary production and available light: Further algorithms for
660 remote sensing. *Deep-Sea Research*, *35*, 855–879. doi:10.1016/0198-0149(88)90064-7.

661 Platt, T., Sathyendranath, S., Forget, M., White, G. N., Caverhill, C., Bouman, H., Devred, E., & Son, S. (2008). Operational estimation of
662 primary production at large geographical scales. *Remote Sensing of Environment*, *112*, 3437–3448. doi:10.1016/j.rse.2007.11.018.

663 Platt, T., Sathyendranath, S., & Ravindran, P. (1990). Primary production by phytoplankton: Analytic solutions for daily rates per unit area
664 of water surface. *Proceeding of the Royal Society B*, *241*, 101–111. doi:10.1098/rspb.1990.0072.

665 Platt, T., Sathyendranath, S., White, G. N., Jackson, T., Saux Picart, S., & Bouman, H. (2017). Primary production: Sensitivity to surface
666 irradiance and implications for archiving data. *Frontiers in Marine Science*, *4*, 387. doi:10.3389/fmars.2017.00387.

667 Prezelin, B. B., Putt, M., & Glover, H. E. (1986). Diurnal patterns in photosynthetic capacity and depth-dependent photosynthesis–irradiance
668 relationships in *synechococcus* spp. *Marine Biology*, *92*, 205–217. doi:10.1007/BF00569436.

669 Reynolds, C. S. (2006). *Ecology of phytoplankton*. (1st ed.). Cambridge University Press. doi:10.1017/CBO9780511542145.

670 Richardson, K., Bendtsen, J., Kragh, T., & Mousing, E. A. (2016). Constraining the distribution of photosynthetic parameters in the global
671 ocean. *Frontiers in Marine Science*, *3*, 1–13. doi:10.3389/fmars.2016.00269.

672 Ross, O. N., Geider, R. J., Berdalet, E., Artigas, M. L., & Piera, J. (2011a). Modelling the effect of vertical mixing on bottle incubations for
673 determining in situ phytoplankton dynamics. i. growth rates. *Marine Ecology Progress Series*, *435*, 13–31. doi:10.3354/meps09193.

674 Ross, O. N., Geider, R. J., & Piera, J. (2011b). Modelling the effect of vertical mixing on bottle incubations for determining in situ
675 phytoplankton dynamics. ii. primary production. *Marine Ecology Progress Series*, *435*, 33–45. doi:10.3354/meps09194.

676 Sakshaug, E., Bricaud, A., Dandonneau, Y., Falkowski, P. G., Kiefer, D. A., Legendre, L., Morel, A., Parslow, J., & Takahashi, M.
677 (1997). Parameters of photosynthesis: definitions, theory and interpretation of results. *Journal of Plankton Research*, *19* (11), 1637–
678 1670. doi:10.1093/plankt/19.11.1637.

679 Sathyendranath, S., & Platt, T. (1989a). Computation of aquatic primary production: Extended formalism to include the effect of angular
680 and spectral distribution of light. *Limnology and Oceanography*, *34*, 188–198. doi:10.4319/lo.1989.34.1.0188.

681 Sathyendranath, S., & Platt, T. (1989b). Remote sensing of ocean chlorophyll: consequence of nonuniform pigment profile. *Applied Optics*,
682 *28*(3), 490–495. doi:10.1364/AO.28.000490.

683 Sathyendranath, S., & Platt, T. (2007). Spectral effects in bio-optical control on the ocean system. *Oceanologia*, *49*, 5–39.

684 Schofield, O., Prezelin, B. B., Smith, R. C., Stegmann, P. M., Nelson, N. B., Lewiss, M., & Baker, K. S. (1991). Variability in spectral and non-
685 spectral measurements of photosynthetic light utilization efficiencies. *Marine Ecology Progress Series*, *78*, 253–271. doi:10.3354/meps078253.

686 Strickland, J. D. H., & Parsons, T. R. (1972). *A practical handbook on seawater analysis*. Fisheries research Board of Canada.
687 doi:10.1002/iroh.19700550118.

688 Topliss, B. J., & Platt, T. (1986). Passive fluorescence and photosynthesis in the ocean: implications for remote sensing. *Deep-Sea Research*,
689 *33*(7), 849–864. doi:10.1016/0198-0149(86)90001-4.

690 Westberry, T. K., Silsbe, G. M., & Behrenfeld, M. J. (2023). Gross and net primary production in the global ocean: An ocean color remote
691 sensing perspective. *Earth-Science Reviews*, *104*322, 1–15. doi:10.1016/j.earscirev.2023.104322.

692 Wu, J., Lee, Z., Goes, J., do Rosario Gomes, H., & Wei, J. (2024). Evaluation of three contrasting models in estimating primary production
693 from ocean color remote sensing using long-term time-series data at oceanic and coastal sites. *Remote Sensing of Environment*, *302*, 113983.
694 doi:10.1016/j.rse.2023.113983.

695 Zheng, Q., Viljoen, J. J., Sun, X., Kovač, S., Sathyendranath, S., & Brewin, R. J. W. (2025). Simulating vertical phytoplankton dynamics in a
696 stratified ocean using a two-layered ecosystem model. *Biogeosciences*, *22*, 3253–3278. doi:10.5194/bg-22-3253-2025.

697 Zonneveld, C. (1997). Modeling effects of photoadaptation on the photosynthesis-irradiance curve. *Journal of Theoretical Biology*, *186*,
698 381–388.

699 Zonneveld, C. (1998). Light-limited microalgal growth: A comparison of modelling approaches. *Ecological Modelling*, *113*, 41–54.
700 doi:10.1016/S0304-3800(98)00133-1.